

Solid-phase room-temperature decomposition of a complex salt *trans*-[Rh(γ -Pic)₄Cl₂]MnO₄

Anatoliy B. Venediktov*, Danila B. Vasilchenko, Irina V. Yushina, Tatyana I. Nedoseykina, Evgeniy Yu. Filatov, Sergey V. Korenev

Nikolaev Institute of Inorganic Chemistry SB RAS, 630090 Novosibirsk, Russia

ARTICLE INFO

Article history:

Received 11 December 2010

Accepted 20 January 2011

Keywords:

Rhodium complexes

Picoline

Permanganate

Manganese dioxide

Nanoparticles

Nanoalloys

ABSTRACT

Permanganate salt of the complex cation *trans*-[Rh(γ -Pic)₄Cl₂]⁺ (γ -Pic = γ -picoline) was synthesized. The unusual decomposition reaction of the salt was studied at room temperature. This process has been found to conserve the γ -picoline ligands in cation untouched. A number of transformations in anionic part of salt have been observed. Metallic products of the salt thermal decomposition have been studied.

© 2011 Elsevier Ltd. All rights reserved.

1. Introduction

Complexes of rhodium(III) with pyridine and its substituted derivatives are of large interest in different branches of chemical science due to their unusual and useful properties. Such complexes are precursors of active catalysts for water–gas shift, hydrogenation, hydroformylation, carbonylation of methanol and other related reactions [1]. Unprecedented antibacterial and antitumor activity was found for the complexes of rhodium(III) with methylpyridines [2]. *Trans*-[RhL₄Cl₂]⁺ cations (L = Py or γ -picoline) appeared useful for isolation of unusual anionic species in the form of stable adducts [3]. In our recent work [4] the cation *trans*-[Rh(γ -Pic)₄Cl₂]⁺ was used for examination of methyl group oxidation in coordinated γ -picoline without destruction of the [RhN₄Cl₂] coordination core. This oxidation was carried out with KMnO₄ as the oxidant, and a poorly soluble salt *trans*-[Rh(γ -Pic)₄Cl₂]MnO₄ is initially formed, which rapidly decomposes in boiling solution. The decomposition of the salt was observed under darkroom conditions at room temperature as well. Several ways for decomposition of MnO₄⁻ are known for solid salts involving both complex and simple inorganic cations, but they require either thermal- [5] or photoactivation [6] to achieve high reaction rate. Therefore, the above-mentioned rapid decomposition of *trans*-[Rh(γ -Pic)₄Cl₂]MnO₄ requires deeper study to understand the nature of such instability.

In the present work, we have studied an uncommon solid-state room-temperature decomposition reaction of aforesaid permanganate salt. In addition, final products of thermal decomposition of the salt have been studied.

2. Experimental

The salt [Rh(γ -Pic)₄Cl₂]Cl·2.5H₂O was prepared by the method described previously [4] from commercial ‘rhodium chloride’ of composition RhCl₃·3H₂O. All employed solvents and reagents were of analytical grade and were used without further purification. Elemental CHN-analyses were performed with Euro EA 3000 analyzer.

Solid state IR spectra were measured with a Scimitar FTS 2000 (4000–400 cm⁻¹, KBr pellets) spectrometer and Vertex 80 IR-FT spectrometer (400–100 cm⁻¹, PE pellets).

UV–Vis spectra were recorded with a Shimadzu UV-3101 PC spectrometer. Diffuse reflectance spectroscopy was carried out with Shimadzu UV–Vis–NIR spectrometer UV-3101 PC using BaSO₄ as a reference. The reflectance spectra were recorded in 240–800 nm range.

A Bruker AVANCE 500 (AV500) spectrometer was used in order to obtain ¹³C nuclear resonance spectra with d₆-acetone as a reference.

Differential thermal analysis of the synthesized compound was carried out with a TG 209 F1 Iris® (NETZSCH) in He stream (70 ml/min) at heating rate 10 K/min.

X-ray diffraction study of polycrystalline samples was carried out on DRON-SEIFERT-RM4 diffractometer (Cu K α – radiation

* Corresponding author. Tel.: +7 383 3165633; fax: +7 383 3309489.

E-mail address: venedik@niic.nsc.ru (A.B. Venediktov).

($\lambda = 1.5418 \text{ \AA}$), graphite monochromator on the diffracted beam, scintillation detector with amplitude discrimination) in 2θ range $5\text{--}60^\circ$. The samples were prepared by deposition of a suspension in hexane on the polished side of a quartz sample holder. Similarly prepared polycrystalline quartz sample ($a = 5.4309 \text{ \AA}$) was used as an external standard. Indexing of the diffraction patterns for the products of thermolysis was carried out using the data for pure metals and compounds reported in the PDF database [7], 2θ range $5\text{--}120^\circ$ was used. Unit cell parameters were refined by the full-profile technique within the whole diffraction range with the POWDERCELL 2.4 program [8].

Mn K-edge XAFS spectrum of MnO_2 was measured in transmission mode at Kurchatov centre of synchrotron radiation (Moscow, Russia). IFFEFIT program suite [9,10] was used for treatment of the XAFS data. Fitting was done in R -space in the range from 1.0 to 3.0 \AA . EXAFS fit was performed simultaneously in k -weightings of one, two and three to avoid errors in coordination numbers and Debye–Waller factors.

Surface morphologies of the materials were studied using a transmission electron microscope JEOL JEM-100CX and scanning electron microscope JSM 6700F with EDS EX-23000 BU.

2.1. $[\text{Rh}(\gamma\text{-Pic})_4\text{Cl}_2]\text{MnO}_4$

Aqueous saturated solution of KMnO_4 was added dropwise to $\sim 0.01 \text{ M}$ solution of $[\text{Rh}(\gamma\text{-Pic})_4\text{Cl}_2]\text{Cl}\cdot 2.5\text{H}_2\text{O}$ at room temperature. The dark-pink precipitate appeared immediately. Addition of KMnO_4 was stopped when the mother liquor turned to pale-pink. The precipitate was collected by filtration, washed with H_2O and Et_2O and dried in air stream (15 min). The yield of the reaction was ca. 98%. Dry salt was kept in darkness at 0°C . The compound is slightly soluble in water, readily soluble in ethanol and acetone, but substantially reacts with them. IR (KBr): $3083(\nu_{\text{C-H}})$, $3047(\nu_{\text{C-H}})$, $2956(\nu_{\text{C-H}})$, $2922(\nu_{\text{C-H}})$, $1621(\nu_{\text{C=N}})$, $1503(\nu_{\text{C=C}})$, $1444(\nu_{\text{C=C}})$, $1433(\nu_{\text{C=C}})$, $1370(\nu_{\text{C=C}})$, $1336(\nu_{\text{C=C}})$, $1237(\delta_{\text{C-H}})$, $1212(\delta_{\text{C-H}})$, $1115(\delta_{\text{C-H}})$, $1064(\delta_{\text{C-H}})$, $1041(\delta_{\text{C-H}})$, $902(\nu_3(\text{MnO}_4^-))$, $813(\gamma_{\text{C-H}})$, $719(\gamma_{\text{C-H}})$, $559(\delta_{\text{ring}})$, $508(\delta_{\text{ring}})$.

Due to the decomposition reaction during the crystallization our attempts to grow a single crystal of the salt were unsuccessful therefore all synthesized and studied samples of $[\text{Rh}(\gamma\text{-Pic})_4\text{Cl}_2]\text{MnO}_4$ are powders of plate crystals with size of ca. $5\text{--}10 \mu\text{m}$ (SEM, Fig. 1).

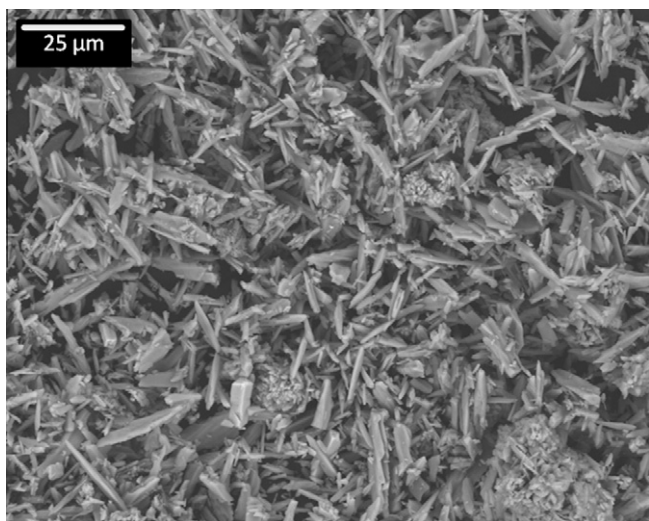


Fig. 1. The SEM image of $[\text{Rh}(\gamma\text{-Pic})_4\text{Cl}_2]\text{MnO}_4$ salt powder.

2.2. $[\text{Rh}(\gamma\text{-Pic})_4\text{Cl}_2]\text{HCO}_3$

To water solution of $[\text{Rh}(\gamma\text{-Pic})_4\text{Cl}_2]\text{Cl}\cdot 2.5\text{H}_2\text{O}$ ($\sim 0.01 \text{ M}$) was added quintuple excess of sodium hydrocarbonate. Pale yellow precipitate was filtered out, recrystallized from acetone, washed with Et_2O . Air-dry salt was kept in dessicator (with conc. H_2SO_4) 48 h to obtain anhydrous product. Yield: 90%. IR (KBr): $3080(\nu_{\text{C-H}})$, $3051(\nu_{\text{C-H}})$, $2953(\nu_{\text{C-H}})$, $2919(\nu_{\text{C-H}})$, $1621(\nu_{\text{C=N}})$, $1608(\nu_{\text{C=O}})$, $1509(\nu_{\text{C=C}})$, $1439(\nu_{\text{C=C}})$, $1433(\nu_{\text{C=C}})$, $1371(\nu_{\text{C=C}})$, $1360(\text{HCO}_3^-)$, $1333(\nu_{\text{C=C}})$, $1232(\delta_{\text{C-H}})$, $1214(\delta_{\text{C-H}})$, $1117(\delta_{\text{C-H}})$, $1061(\delta_{\text{C-H}})$, $1037(\delta_{\text{C-H}})$, $810(\gamma_{\text{C-H}})$, $722(\gamma_{\text{C-H}})$, $703(\text{HCO}_3^-)$, $565(\delta_{\text{ring}})$, $512(\delta_{\text{ring}})$. Anal. Calc. for $\text{C}_{25}\text{H}_{29}\text{Cl}_2\text{N}_4\text{O}_3\text{Rh}$: C, 49.44; H, 4.81; N, 9.22. Found: C, 49.32; H, 8.9; N, 9.1%.

3. Results and discussion

3.1. The room-temperature decomposition process

Addition of KMnO_4 to solution of the $[\text{Rh}(\gamma\text{-Pic})_4\text{Cl}_2]\text{Cl}\cdot 2.5\text{H}_2\text{O}$ results in precipitation of low-soluble salt $[\text{Rh}(\gamma\text{-Pic})_4\text{Cl}_2]\text{MnO}_4$. Due to the decomposition reaction during the crystallization our attempts to grow a single crystal of the salt were unsuccessful therefore all synthesized and studied samples of $[\text{Rh}(\gamma\text{-Pic})_4\text{Cl}_2]\text{MnO}_4$ are powders of plate crystals (Fig. 1) with size of ca. $5\text{--}10 \mu\text{m}$. Powder diffraction pattern of the salt was indexed using earlier published single crystal data for isostructural $[\text{Rh}(\gamma\text{-Pic})_4\text{Cl}_2]\text{ReO}_4$ [4]. Unit cell parameters were refined by the full-profile technique using all diffraction data with Rietveld–Toraya (plate, according to SEM) preferred orientation model for (0 1 1) plane (Fig. 2). Cell parameters for permanganate salt (space group $P2_1/c$, $a = 11.804(4) \text{ \AA}$, $b = 11.260(4) \text{ \AA}$, $c = 21.762(8) \text{ \AA}$, $\beta = 103.88(3)^\circ$, $V = 2800.9(4) \text{ \AA}^3$) are less than parameters of $[\text{Rh}(\gamma\text{-Pic})_4\text{Cl}_2]\text{ReO}_4$ salt ($a = 11.866$, $b = 11.296$, $c = 22.049$, $\beta = 104.10^\circ$, $V = 2866.4 \text{ \AA}^3$) due to smaller ion radius of manganese versus rhenium.

Permanganate salt at room temperature gradually decomposes with formation of a brown substance. Decomposition occurs both in daylight and in darkness. The process is accompanied by notable spectral changes. The evolution of electronic spectrum for a sample of the salt during 24 h ($T = 20 \pm 1^\circ\text{C}$) is shown in Fig. 3.

The bands of MnO_4^- ion in the region $480\text{--}600 \text{ nm}$ disappear and a broad band at $320\text{--}390 \text{ nm}$ with a shoulder around 500 nm is formed. Analogous broad band with shoulder around 500 nm

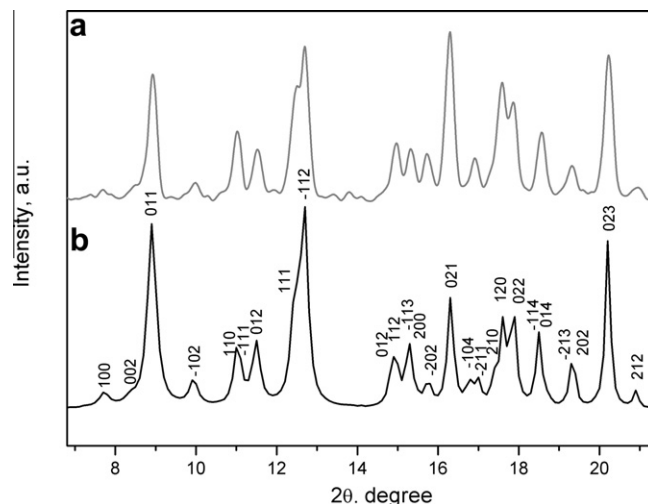


Fig. 2. Diffraction patterns of $[\text{Rh}(\gamma\text{-Pic})_4\text{Cl}_2]\text{MnO}_4$ with indexing according to $[\text{Rh}(\gamma\text{-Pic})_4\text{Cl}_2]\text{ReO}_4$ crystal structure.

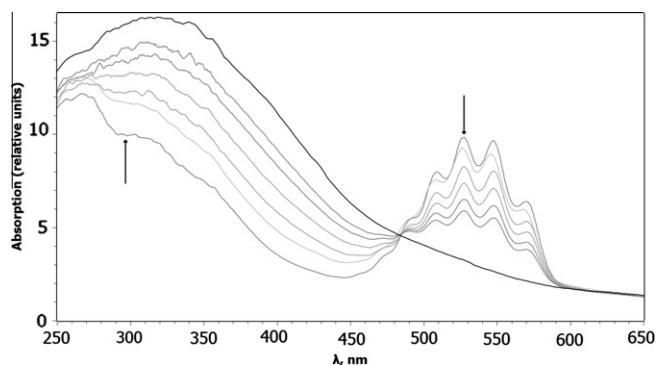


Fig. 3. The diffuse reflectance UV–Vis spectra change of $[\text{Rh}(\gamma\text{-Pic})_4\text{Cl}_2]\text{MnO}_4$ during the decomposition process. The spectra were recorded after 1, 2, 3, 4, 5, 6 and 12 h from precipitation of the salt.

were observed in spectra of MnO_2 and assigned to the charge transfer band superimposed on ${}^5\text{B}_{1g} \rightarrow {}^5\text{B}_{2g}$ and ${}^5\text{B}_{1g} \rightarrow {}^5\text{E}_g$ d–d transitions [11]. There is no evidence of manganate-ion absorption band in the spectra, thus decomposition of $[\text{Rh}(\gamma\text{-Pic})_4\text{Cl}_2]\text{MnO}_4$ has different nature than in the case of alkali and alkali-earth metals permanganates [5d]. The evolution of intensities of both absorption bands (growth for MnO_2 band and decrease for MnO_4^- bands) obey the exponential law Fig. 4. Similar changes may be found in IR spectra of the salt during its decomposition. The band at 902 cm^{-1} ($\nu_3(\text{MnO}_4^-)$) disappears and a broad band in $550\text{--}400\text{ cm}^{-1}$ region arises. In addition, a strong broad band appears at 3400 cm^{-1} . Initial diffraction pattern of $[\text{Rh}(\gamma\text{-Pic})_4\text{Cl}_2]\text{MnO}_4$ during first 8–10 h of the decomposition process survives but practically all peaks shift in small-angle range for ca. 0.4° (Fig. 5). Further evolution of decomposition process results in formation of totally X-ray-amorphous powder with diffuse broad peaks like it takes place in case of fully amorphous products of AgMnO_4 decomposition at 110°C [5d]. Aforesaid peaks shift suggests significant increasing of interplanar spacings and unit cell volume of source salt before full collapse. In addition it should be noted that $[\text{Rh}(\gamma\text{-Pic})_4\text{Cl}_2]\text{MnO}_4$ salt prepared from $[\text{Rh}(\gamma\text{-Pic})_4\text{Cl}_2]\text{NO}_3$ undergoes the same transformation with identical rate.

In order to investigate the processes taking place during decomposition of the permanganate salt, an experiment with the

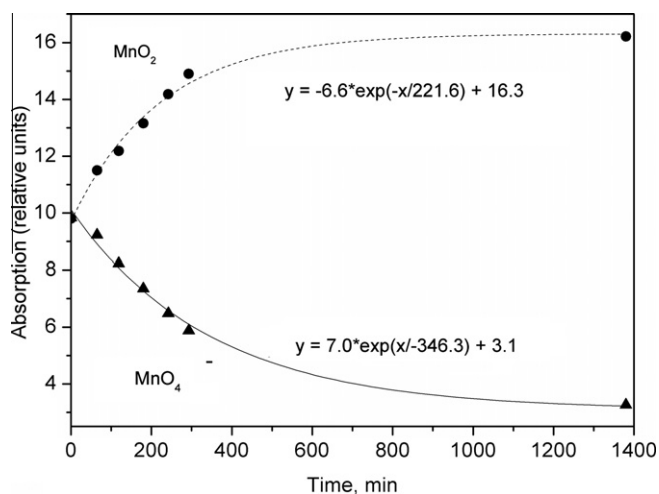


Fig. 4. Showing of course of adsorption maxima at 300 (MnO_2) and 527 nm (MnO_4^-) during the salt decomposition process.

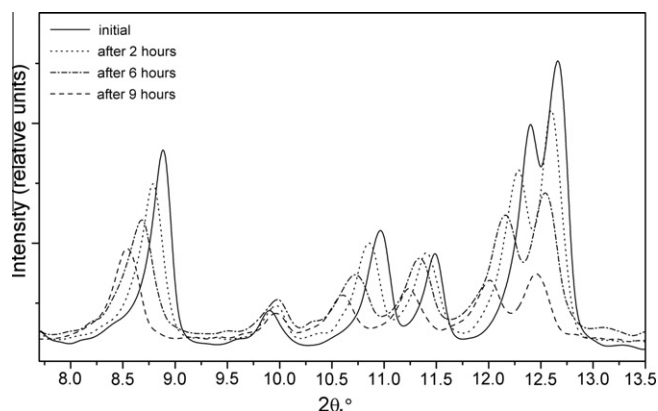
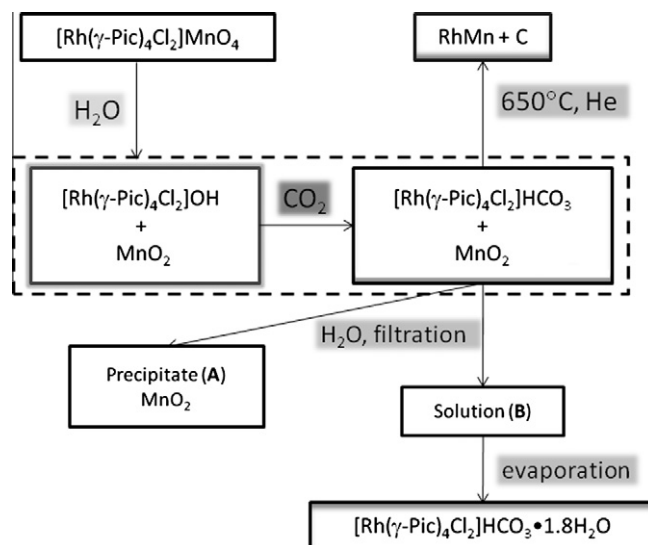


Fig. 5. Diffraction patterns evolution of $[\text{Rh}(\gamma\text{-Pic})_4\text{Cl}_2]\text{MnO}_4$ during initial period of the decomposition process (only $2\theta = 8\text{--}13^\circ$ range is shown for clarity).

brown residue was carried out (Scheme 1). A sample of the brown residue obtained on decomposition of the initial salt at room temperature during 2 days was stirred in hot (60°C) water for about 40 min, a dark-brown precipitate (A) was filtered off and the resulting solution (B) (pH 10) was evaporated until yellow platelet crystals formed. The crystals were collected by filtration, washed with icy water and dried. The IR-spectrum of this compound is close to that of $[\text{Rh}(\gamma\text{-Pic})_4\text{Cl}_2]\text{Cl}\cdot 2.5\text{H}_2\text{O}$ with exception for adsorption bands at 1606 , 1361 and 700 cm^{-1} , also observed in the IR spectrum of the decomposition product (Fig. 6). The first one overlaps with the band of C–N stretching vibrations. The described bands are observed in spectra of hydrocarbonates and were assigned to stretching vibration in HCO_3^- anions [12]. These addition IR-bands miss if CO_2 -free atmosphere is used during the decomposition. Elemental analysis gives reasons to consider the obtained compound as hydrocarbonate due to good agreement with $[\text{Rh}(\gamma\text{-Pic})_4\text{Cl}_2]\text{HCO}_3\cdot 1.8\text{H}_2\text{O}$ composition (Anal. Calc. C, 46.94; H, 5.13; N, 8.76. Found: C, 46.9; H, 5.0; N, 9.2%). Titration of the compounds with 0.1 M hydrochloric acid gives a typical single-step titration curve of a hydrocarbonate salts (equivalence points is about pH 4). Aforesaid hydrocarbonate formula was confirmed by determination of the molecular mass of this compound based on measured extinction of $[\text{Rh}(\gamma\text{-Pic})_4\text{Cl}_2]^+$ at 402 nm ($86.8\text{ l mol}^{-1}\text{ cm}^{-1}$). The value deviates from theoretical for



Scheme 1. Sequence of transformation of the permanganate salt described in the paper. Products of the room-temperature decomposition are shown in dash box.

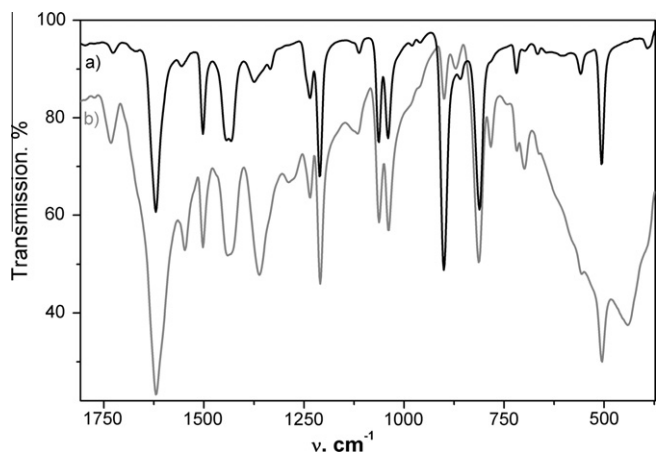


Fig. 6. IR-spectra of $[\text{Rh}(\gamma\text{-Pic})_4\text{Cl}_2]\text{MnO}_4$ (a) and product of its decomposition (b).

$[\text{Rh}(\gamma\text{-Pic})_4\text{Cl}_2]\text{HCO}_3 \cdot 1.8\text{H}_2\text{O}$ on 5%, what can be attributed to both instrumental errors and variable hydrate number of the salt. XRD pattern of the hydrocarbonate salt samples depends markedly on its hydrate composition. Diffraction pattern of anhydrous powder is identical to authentic $[\text{Rh}(\gamma\text{-Pic})_4\text{Cl}_2]\text{HCO}_3$ pattern with the exception of better crystallinity of the latter.

^{13}C NMR spectrum of solution (B) is identical to the spectrum of $[\text{Rh}(\gamma\text{-Pic})_4\text{Cl}_2]^+$ cation (20.86 ppm ($-\text{CH}_3$), 126.68 ppm (C2), 152.86 ppm (C3), 154.13 ppm (C1)) and does not contain additional signals. Therefore in three experiments solution (B) was treated with excess of NaReO_4 and low-soluble $[\text{Rh}(\gamma\text{-Pic})_4\text{Cl}_2]\text{ReO}_4$ (identified by XRD, CHN and IR-spectroscopy) was precipitated. Quantity of $[\text{Rh}(\gamma\text{-Pic})_4\text{Cl}_2]^+$ cation precipitated in this form corresponds with 99% of its initial amount in $[\text{Rh}(\gamma\text{-Pic})_4\text{Cl}_2]\text{MnO}_4$ (98.7%, 99.1%, 99.4% in three particular experiments).

Insoluble dark-brown precipitate (A) is amorphous, and to study its structure XAFS-spectroscopy [13] was applied. Fourier transforms (FT) of the experimental and theoretically calculated Mn K-edge $k^2\chi(k)$ spectra for the sample are shown in Fig. 7. The two strong FT peaks centred at 1.5 and 2.5 Å (phase shift uncorrected) represent Mn–O and Mn–Mn coordination shells. According to the data obtained from the fitting procedure, 5.6(5) oxygen and 3.8(4) manganese atoms occur in the shells with radii 1.899(5) Å and 2.890(9) Å, respectively. Debye–Waller factor is $0.0026(6)\text{Å}^2$ for Mn–O and $0.006(1)\text{Å}^2$ for Mn–Mn.

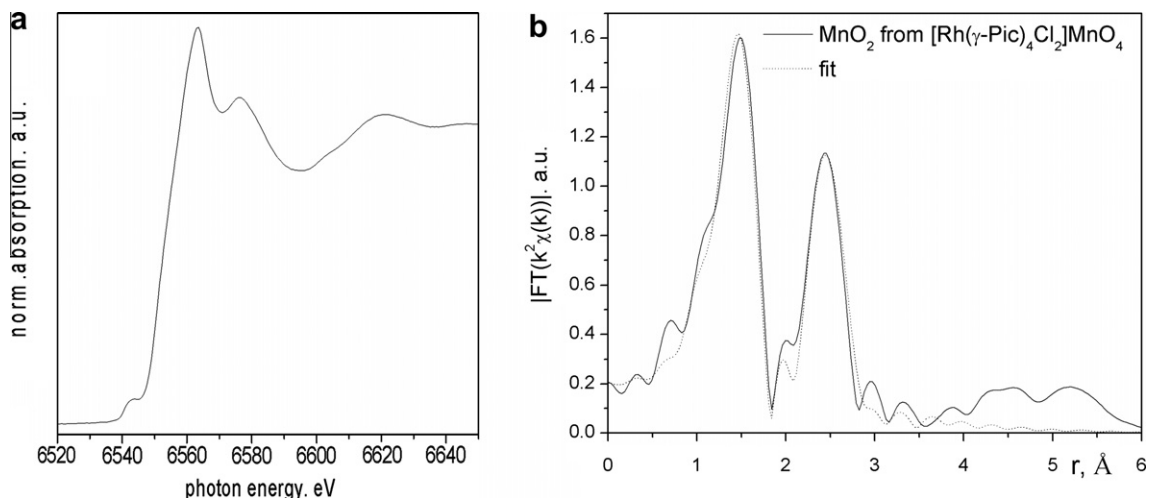
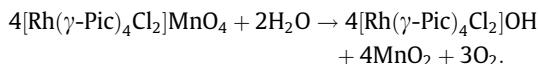


Fig. 7. Mn K-edge XANES spectrum (a) and Fourier transform of k^2 -weighted EXAFS spectrum fitted with FEFF7 theory (---) to the data (---) of sample MnO_2 obtained from $[\text{Rh}(\gamma\text{-Pic})_4\text{Cl}_2]\text{MnO}_4$ salt (b).

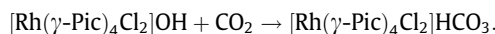
EXAFS-parameters for the sample are very similar to those for an electrodeposited manganese oxide [11].

$[\text{Rh}(\gamma\text{-Pic})_4\text{Cl}_2]\text{MnO}_4$ slowly decomposes in several weeks when kept in vacuum. Product of vacuum decomposition exhibits several extra bands in IR-spectrum in comparison with IR-spectrum of air-decomposed salt. These bands lie in region of the C–H and the C–C bonds stretching vibration of $\gamma\text{-Pic}$ and so can be assigned with product of ligand oxidation.

Thus, during solid-state room-temperature $[\text{Rh}(\gamma\text{-Pic})_4\text{Cl}_2]\text{MnO}_4$ decomposition MnO_4^- ion is reduced to MnO_2 . On the other hand, the presence of HCO_3^- ion indicates the formation of OH^- capturing CO_2 from air. Under such conditions the following equation of the decomposition process seems probable:



However, vacuum decomposition experiment shows what oxidation of coordinated picoline takes place but it is low-rate process in comparison with rate of water-induced reaction. Absorption of CO_2 from air by $[\text{Rh}(\gamma\text{-Pic})_4\text{Cl}_2]\text{OH}$ is trivial:



Characterisation of $[\text{Rh}(\gamma\text{-Pic})_4\text{Cl}_2]\text{OH}$ is complicated due to absence of diffraction pattern from samples of this compound and easy picoline loss via substitution reaction. Thus CO_2 capturing with formation of the hydrocarbonate salt is useful situation for detection and separation of rhodium complex from the decomposition products.

Water molecules participating in decomposition process are the water adsorbed onto the surface of the crystals or are the water of crystallization. It is difficult to prevent the admixture of such small amount of water (about 1 mass% for complete decomposition) during preparation of the salt. Thus, at ambient temperature the salt decomposes even when stored in a desiccator.

The composite material formed after room-temperature decomposition of $[\text{Rh}(\gamma\text{-Pic})_4\text{Cl}_2]\text{MnO}_4$ was examined with TEM. As one can see from Fig. 8, nanoparticles of MnO_2 with size about 2–3 nm are uniformly distributed in the matrix of the complex. This matrix provides the stability of the oxide particles of such small size. The selected-area electron diffraction (SAED) patterns display several regular highlighted diffraction spots with $d = 2.1$ and 2.8 Å which can be indexed to $\beta\text{-MnO}_2$. Thus MnO_4^- anions from source salt after decomposition form particle of MnO_2 phase

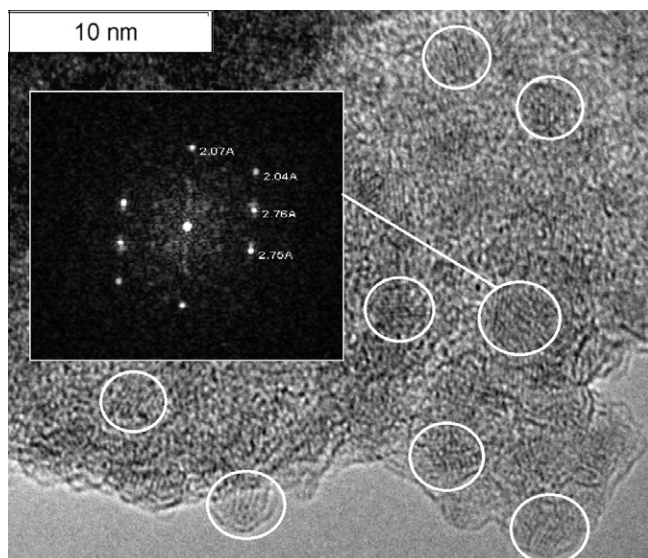


Fig. 8. The TEM image of decomposition products of $[\text{Rh}(\gamma\text{-Pic})_4\text{Cl}_2]\text{MnO}_4$ salt. MnO_2 nanoparticles are shown in white circles.

and this process has to be accompanied with intensive diffusion of Mn-containing particles.

It appears that the reason of $[\text{Rh}(\gamma\text{-Pic})_4\text{Cl}_2]\text{MnO}_4$ reactivity is the high dispersion of salt samples and big free volume in structure of salt (packing fraction is about 0.39) simplifying diffusion processes during the decomposition.

3.2. A thermally induced decomposition

The rate of decomposition of the permanganate salt strongly depends on temperature. Heating of the salt up to 60 °C results in rapid (5–10 s) change of its dark-pink colour into brown. Further

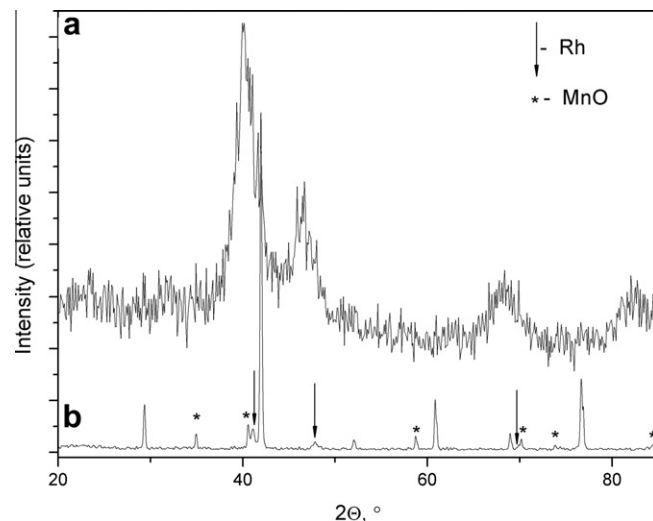


Fig. 9. Diffraction pattern of $\text{Rh}_x\text{Mn}_{1-x}$ solid solution (a) and products of its annealing in hydrogen atmosphere at 650 °C (b).

heating results in destruction of the rhodium tetraamine complex. Thermogram of the salt demonstrates a strong endothermic effect at 100 °C accompanied by the mass change over 40%, and then slow destructive oxidation of coordinated γ -picolinic ligands takes place in 200–400 °C temperature range. Analogous transformations were observed in bis(pyridine)silver(I) permanganate and its pyridine solvate [5a]. Thus, picoline molecules can escape untouched or as the products of its oxidation by MnO_2 or rhodium ions which are reduced to metallic form.

Total mass loss after heating of the salt up to 650 °C is 72%, and the final product of thermolysis is $\text{Rh}_x\text{Mn}_{1-x}$ solid solution ($a = 2.76(1)$ Å, $c = 3.56$ Å, space group $P4/mmm$) and amorphous carbon. Diffuse form of peaks of the XRD pattern (Fig. 9) suggests

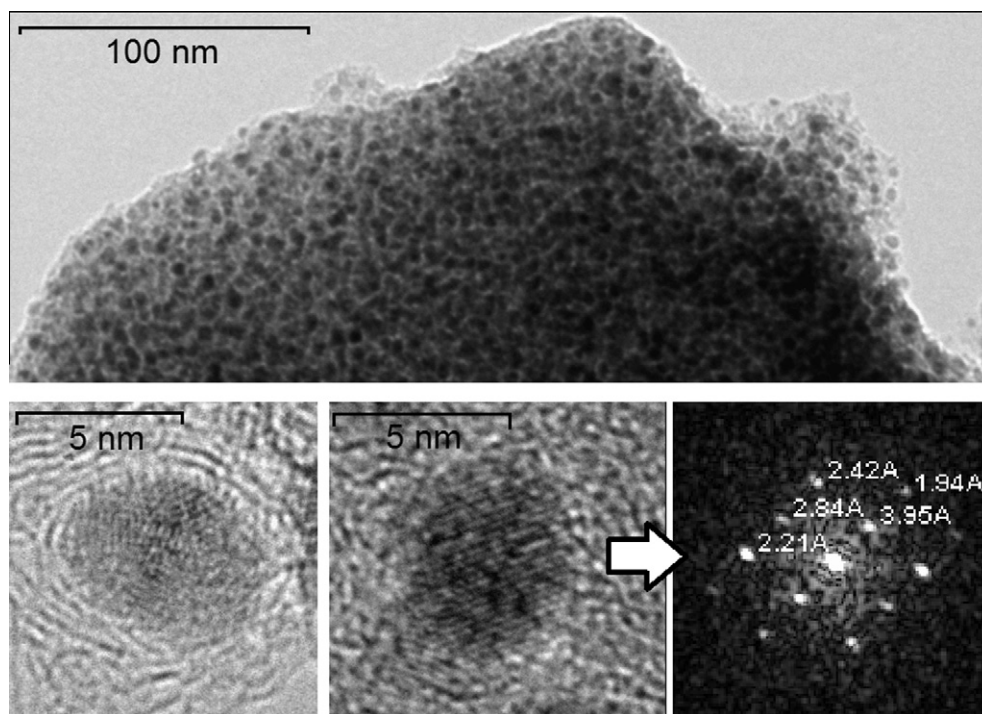


Fig. 10. The TEM images of $\text{Rh}_x\text{Mn}_{1-x}$ solid solution nanoparticles in carbon matrix.

a small size of $\text{Rh}_x\text{Mn}_{1-x}$ particles (3–8 nm). It should be noted that such thermal treatment usually results in sintering of metallic nanoparticles, and, thus, stabilizing effect of carbon was supposed for this case. Similar stabilization by carbon shell was observed for nanoparticles of Co and ZrO_2 metastable phases [14]. TEM photographs of thermal decomposition products fully confirm this hypothesis. Particles of $\text{Rh}_x\text{Mn}_{1-x}$ solid solution are wrapped in carbon sheets (Fig. 10), which prevent sintering of the particles. Overall Rh:Mn ratios given by EDS are close to 1:1. In the SAED patterns for several selected particles diffraction spots can be assigned to Mn_3Rh phase. Particle localised EDS analysis gives Rh:Mn ratio 1:3, thus about 60–70% of rhodium after heating are localised in low-dimension particles of individual phase (Rh^0) or composite (Rh_xC) form.

Annealing of this sample in hydrogen atmosphere at 650 °C during 2 h results in diffusion major part of rhodium into bimetallic particles. According to XRD product of annealing is a multiphase mixture containing $\text{Rh}_{0.4}\text{Mn}_{0.6}$ solid solution ($a = 3.042(2)$ Å, space group $Pm\bar{3}m$) and small amount (<2 mass%) of MnO (aerial oxidation of Mn occurs during removal of sample from reactor) and Rh^0 (Fig. 9).

4. Conclusions

Decomposition of $[\text{Rh}(\gamma\text{-Pic})_4\text{Cl}_2]\text{MnO}_4$ salt at room temperature has been shown to result in formation of a mixture of MnO_2 nanoparticles and $[\text{Rh}(\gamma\text{-Pic})_4\text{Cl}_2]\text{OH}$ complex. Thermal decomposition of the mentioned mixture yields bimetallic particles (3–8 nm) of $\text{Rh}_x\text{Mn}_{1-x}$ solid solution. Using of metal–organic compounds as a precursor for preparation metal and oxide particles is a very popular topic today [15].

It is interesting to notice that after initial decomposition of the salt Mn and Rh atoms are isolated in two different phases MnO_2 and $[\text{Rh}(\gamma\text{-Pic})_4\text{Cl}_2]\text{OH}$, respectively. During heating of this mixture the metals form the phase of $\text{Rh}_x\text{Mn}_{1-x}$ solid solution without melting of components. Metal and oxide particles formed in the decomposition process apparently have extra free energy. This

energy stimulates high diffusion activity of atoms in phase transformations and allows surmounting the energy barrier for growth of a new phase of $\text{Rh}_x\text{Mn}_{1-x}$ solid solution.

The stabilization of such bimetallic nanoparticles by carbon produced in decomposition process occurring in the studied system is a promising pathway to preparation of analogous particles of various metals.

References

- [1] (a) A.J. Pardey, M. Fernandez, M. Canestrari, P. Baricelli, E. Lujano, C. Longo, R. Sartori, S.A. Moya, *React. Kinet. Catal. Lett.* 67 (1999) 325; (b) A. Bakac, *Dalton Trans.* (2006) 1589.
- [2] R.D. Gillard, E. Lekkas, *Transition Met. Chem.* 25 (2000) 617.
- [3] (a) R.D. Gillard, L.R. Hanton, S.H. Mitchell, *Polyhedron* 17 (1990) 2127; (b) R.D. Gillard, S.H. Mitchell, *Polyhedron* 10 (1987) 1885.
- [4] S.V. Korenev, D.B. Vasil'chenko, I.A. Baidina, E.Yu. Filatov, A.B. Venediktov, *Russ. Chem. Bull., Int. Ed.* 57 (2008) 1637.
- [5] (a) L. Kótai, J. Fodor, E. Jakab, I. Sajó, P. Szabó, F. Lónyi, J. Valyon, I. Gárcs, G. Argay, *Transition Met. Chem.* 31 (2006) 30; (b) I.E. Sajó, L. Kótai, G. Keresztury, I. Gács, Gy. Pokol, J. Kristóf, B. Soptrayanov, V.M. Petrusevski, D. Timpu, P.K. Sharma, *Helv. Chim. Acta* 91 (2008) 1646; (c) L. Kótai, K.K. Banerji, I.E. Sajó, J. Kristóf, B. Sreedhar, S. Holly, G. Keresztury, A. Rockenbauer, *Helv. Chim. Acta* 85 (2002) 2316; (d) F.H. Herbstein, M. Kapon, A. Weissman, *J. Therm. Anal.* 41 (1991) 303.
- [6] H. Nakai, Y. Ohmori, H. Nakatsuji, *J. Phys. Chem.* 99 (1995) 8550.
- [7] Powder Diffraction File, Alphabetical Index, Inorganic Phases, JCPDS, International Centre for Diffraction Data, Pennsylvania, USA, 1983.
- [8] G. Nolze, W. Kraus, *Powder Diffr.* 13 (1998) 256.
- [9] B. Ravel, M. Newville, *J. Synchrotron Rad.* 12 (2005) 537.
- [10] M. Newville, *J. Synchrotron Rad.* 8 (2001) 322.
- [11] K.-W. Nam, M.G. Kim, K.-B. Kim, *J. Phys. Chem. C* 111 (2007) 749.
- [12] K. Nakamoto, *IR Spectra of Inorganic and Coordination Compounds*, fifth ed., Wiley, New York, 1997. p. 400.
- [13] D.C. Koningsberger, R. Prins, *X-ray Absorption: Principles, Applications, Techniques of EXAFS, SEXAFS, and XANES*, in *Chemical Analysis*, John Wiley and Sons, 1988. p. 688.
- [14] (a) S.V. Pol, V.G. Pol, G. Seisenbaeva, V.G. Kessler, A. Gedanken, *Chem. Mater.* 16 (2004) 1793; (b) S. Liu, J. Zhu, Y. Mastrai, I. Felner, A. Gedanken, *Chem. Mater.* 12 (2000) 2205.
- [15] O.A. Nikonova, K. Jansson, V.G. Kessler, M. Sunberg, A.I. Baranov, A.V. Shevelkov, D.V. Drobot, G.A. Seisenbaeva, *Inorg. Chem.* 47 (2008) 1295.